Agricultural and Forest Meteorology
Volumes 298–299, 15 March 2021, 108277

Assessing variability of optimum air temperature for photosynthesis across site-years, sites and biomes and their effects on photosynthesis estimation

Qing Chang [a], Xiangming Xiao [a] ✉, Russell Doughty [a], Xiaocui Wu [a], Wenzhe Jiao [b], Yuanwei Qin [a]

https://doi.org/10.1016/j.agrformet.2020.108277

Highlights

- Optimum air temperature of photosynthesis from GPP_{EC} agree well with those from MODIS EVI.
- Optimum air temperature of photosynthesis from GPP_{EC} and MODIS EVI differed substantially from those that are currently used in satellite-based models.
- Use of optimum air temperature of photosynthesis from site-year specific or biome-specific approaches can affects global GPP estimates substantially.

Abstract

Gross primary productivity (GPP) of vegetation is affected by air temperature. Biogeochemical models use the optimum air temperature (T_{opt}) parameter, which comes from biome-specific look-up tables ($\mathbf{T_{opt-b-LT}}$). Many studies have shown that plants have the capacity to adapt to changes in environmental conditions over time, which suggests that the static $\mathbf{T_{opt-b-LT}}$ parameters in the biogeochemical models may poorly represent actual $\mathbf{T_{opt}}$ and induce uncertainty in GPP estimates. Here, we estimated biome-specific, site-year-specific, and site-specific optimum air temperature using GPP data from eddy covariance (EC) flux tower sites (GPP_{EC}) ($\mathbf{T_{opt-b-EC}}$, $\mathbf{T_{opt-sy-EC}}$, $\mathbf{T_{opt-s-EC}}$), the Enhanced Vegetation Index (EVI) from MODIS images ($\mathbf{T_{opt-b-EVI}}$, $\mathbf{T_{opt-sy-EVI}}$, $\mathbf{T_{opt-s-EVI}}$), and mean daytime air temperature (T_{DT}). We evaluated the consistency among the four $\mathbf{T_{opt}}$ parameters ($\mathbf{T_{opt-b}}$, $\mathbf{T_{opt-sy}}$, $\mathbf{T_{opt-s}}$ and $\mathbf{T_{opt-b-LT}}$), and assessed how they affect satellite-based GPP estimates. We find that $\mathbf{T_{opt}}$ parameters from MODIS EVI agree well with those from GPP_{EC}, which indicates that EVI can be used as a variable to estimate $\mathbf{T_{opt}}$ at individual pixels over large spatial domains. $\mathbf{T_{opt-b}}$, $\mathbf{T_{opt-sy}}$, and $\mathbf{T_{opt-s}}$ differed significantly from $\mathbf{T_{opt-b-LT}}$. GPP estimates using $\mathbf{T_{opt-b}}$ and $\mathbf{T_{opt-sy}}$ were more consistent with GPP_{EC} than when using $\mathbf{T_{opt-b-LT}}$ for all the land cover types. Our use of $\mathbf{T_{opt-sy}}$ substantially improved 8-day and annual GPP estimates across biomess (from 1% to 34%), especially for cropland, grassland, and open shrubland. Our simple calculation shows that global GPP estimates differ by up to 10 Pg C/yr when using our

suggested $\mathbf{T_{opt-sy-EVI}}$ instead of using the static $\mathbf{T_{opt-b-LT}}$. Our new approach on estimating T_{opt} has the potential to improve estimates of GPP from satellite-based models, which could lead to better understanding of carbon-climate interactions.

Previous Next

Keywords

Vegetation photosynthesis model; MODIS EVI; Carbon fluxes; Air temperature

1. Introduction

Gross primary production (GPP) of terrestrial vegetation is a critical part of the global carbon cycle and plays a vital role in regulating climate change by sequestering atmospheric CO_2 (Battin et al., 2009; Sitch et al., 2008). The annual GPP of terrestrial vegetation has been estimated to be about 120 Pg C/yr (Haberl et al., 2007; Tutmez, 2006), which is considerably greater than fossil fuel carbon emission (~10 PgC/yr). Thus, small changes in GPP could dramatically affect atmospheric CO_2 concentrations. Accurate GPP estimates are needed for better understanding the global carbon cycle, assessing the response of terrestrial ecosystem to global warming, and forecasting how future changes in climate affect GPP (Anav et al., 2015; Ryu et al., 2019).

Remote sensing provides data essential for understanding terrestrial ecosystems, such as canopy structure, plant photosynthetic capacity, and carbon fluxes (Badgley et al., 2017; Chang et al., 2019; Zhang et al., 2016). There are two major types of data-driven GPP models that use satellite images: (1) GPP models that use statistical algorithms or machine learning and (2) GPP models that use light absorption and light use efficiency (LUE) or radiation use efficiency (RUE) (Monteith, 1972; Potter et al., 2003; Running and Zhao, 2015; Xiao et al., 2004). A comparison of data-driven GPP models showed substantial uncertainties both spatially and temporally (Anav et al., 2015). The trends and interannual variation of annual GPP differ considerably across models (Ryu et al., 2019). A large bias was found between GPP simulated from 26 terrestrial ecosystem models and GPP estimated with eddy covariance (EC) sites in the United States, especially under dry and cold conditions (Schaefer et al., 2012). Several GPP data products have been used to study the response of terrestrial ecosystems to climate variability (Jiao et al., 2019; Wu et al., 2018a; Yang et al., 2019). The differences and uncertainties in satellite-based GPP models have yielded different conclusions about how terrestrial ecosystems respond to increased atmospheric CO_2, warmer mean annual temperatures, and extreme disturbance events (flooding, drought, heatwave) (Stocker et al., 2019; Wu et al., 2018b). Therefore, there is a need to more accurately estimate GPP with models at different spatial scales.

The satellite- and LUE-based GPP models are simple and have been widely used to estimate carbon flux at local, regional, and global scales (Monteith, 1977; Zhang et al., 2016; Zhao and Running, 2010). These GPP models calculate daily GPP as the product of absorbed photosynthetically active radiation (APAR) and LUE ($\boldsymbol{GPP = APAR \times LUE}$) (Monteith, 1972). LUE values in these models are downscaled from maximum LUE (LUE_0) using environmental constraints such as temperature, water, and leaf demography (Pei et al., 2018; Running and Zhao, 2015; Zhang et al., 2017). The relationships between GPP and environmental factors affect the accuracy of GPP estimates (Durgun et al., 2016; Huang et al., 2019; Zheng et al., 2018).

The relationships between GPP and air temperature are commonly described as bell-shaped (Fitter and Hay, 2012; Lin et al., 2012). Here, we define optimum temperature (T_{opt}) as the temperature at which photosynthesis peaks for a given period (e.g., a year) and over a given area (e.g., a pixel). This is different from the maximum photosynthesis that could be achieved in optimal conditions when photosynthesis in unconstrained by environmental conditions. Many GPP models assume a single photosynthesis-air temperature response curve for each biome, and use a biome-specific look-up table, in which maximum, optimum, and minimum air temperature parameters are defined for each biome (Melillo et al., 1993; Running and Zhao, 2015; Turner et al., 2006a; Zhang et al., 2017). A biome (e.g., forest, grassland) is often distributed across large geographical areas and across a gradient of environmental conditions, and plant species in a biome are likely to have adapted to local environmental conditions (Niu et al., 2012; Smith et al., 2016). Furthermore, the parameters set for a given biome, especially for those biomes with large geographic distribution, might not have been collected from a representative sample of observations (McGuire et al., 1992; Raich et al., 1991). For example, eddy flux tower sites are mainly located in the temperate zone in the United States and

Europe. Thus, biome-specific air temperature parameter values in the look-up table cannot capture local photosynthesis-air temperature relationships (Heinsch et al., 2006; Turner et al., 2006b; Yan et al., 2015).

The temperature scalar (T_s) in LUE-based GPP models is particularly sensitive to the choice of optimum air temperature (Zhang et al., 2017). T_{opt} values in most of the GPP models were biome-specific, including MOD17 GPP (Running and Zhao, 2015), VPM (Xiao et al., 2004), TEC (Yan et al., 2015), C-Fix (Veroustraete et al., 2002), EC-LUE (Yuan et al., 2007), CFLUX (King et al., 2011), and GLO-PEM (Prince and Goward, 1995). A recent study suggested that the biome-specific T_{opt} values used in the models were much higher than under natural conditions (Huang et al., 2019). Here, we used biome-specific ($T_{opt\text{-}b}$), site-specific ($T_{opt\text{-}s}$), and site-year-specific ($T_{opt\text{-}sy}$) optimum temperature to estimate GPP for comparison to GPP_{EC}. The site-year-specific optimum temperature parameters ($T_{opt\text{-}sy}$) vary among sites across years and are different than the biome-specific temperature parameters ($T_{opt\text{-}b}$).

The global network of eddy covariance flux tower sites provides GPP (GPP_{EC}) and air temperature (T_{EC}) data, and are often used to quantify the photosynthesis-related temperature parameters at the ecosystem or landscape scales (Baldocchi, 2003). Here, we used the EC data to compare $T_{opt\text{-}sy}$, T_{opt_s} and $T_{opt\text{-}b}$ at the site scale. However, it is important to note that there is a limited number of EC towers in the world (Anav et al., 2015) . Therefore, there is a need to explore satellite data for a proxy that could be used to approximate the photosynthesis-temperature relationship, specifically, $T_{opt\text{-}s}$ or $T_{opt\text{-}sy}$.

Vegetation indices (VIs) are used as satellite proxies for photosynthesis in many studies (Gamon et al., 2013; Yan et al., 2019). The commonly used VIs includes the Enhanced Vegetation Index (EVI) and the Normalized Difference Vegetation Index (NDVI). Compared to NDVI, EVI is less affected by atmospheric conditions and soil background, and is a better proxy of canopy chlorophyll content and canopy greenness than NDVI because NDVI tends to saturate when leaf area index is high (Chang et al., 2019; Huete et al., 2002). EVI is significantly correlated with FPAR, APAR, and GPP (Ma et al., 2014; Zhang et al., 2017). To date, there are few studies that investigate the use of EVI to estimate $T_{opt\text{-}s}$ and $T_{opt\text{-}sy}$ (Chang et al., 2020; Huang et al., 2019).

Several studies sought to improve GPP estimates by adjusting $T_{opt\text{-}b}$, and found that uncertainties in GPP estimates could be reduced by adjusting the optimized parameters in GPP models using eddy covariance CO_2 flux observations (Xiao et al., 2014; Xiao et al., 2011). Several studies suggested that the use of biome-specific temperature parameters ($T_{opt\text{-}b}$), rather than site-year-specific temperature parameters ($T_{opt\text{-}sy}$), introduced some uncertainties in GPP estimates (Heinsch et al., 2006; Turner et al., 2006b; Yan et al., 2015). A comprehensive study to assess the effect of $T_{opt\text{-}b}$, $T_{opt\text{-}s}$, and $T_{opt\text{-}sy}$ in GPP models could help improve the estimates of GPP. To date, no study has used EC tower sites to assess the effect of $T_{opt\text{-}b}$, $T_{opt\text{-}s}$, and $T_{opt\text{-}sy}$ on GPP estimates in the GPP models.

To address the need to improve the optimum air temperature parameter estimates, our objectives were to: 1) estimate $T_{opt\text{-}sy}$, $T_{opt\text{-}s}$ and $T_{opt\text{-}b}$ by using GPP_{EC} and air temperature data from EC flux tower sites ($\mathbf{T_{opt-b-EC}}$, $T_{opt\text{-}s\text{-}EC}$, $\mathbf{T_{opt-sy-EC}}$) and quantify their differences to $T_{opt\text{-}b}$ from the Biome Property Look-up Table ($\mathbf{T_{opt-b-LT}}$); 2) estimate $T_{opt\text{-}sy}$, $T_{opt\text{-}s}$, and $T_{opt\text{-}b}$ by using EVI and air temperature data ($\mathbf{T_{opt-sy-EVI}}$, $T_{opt\text{-}s\text{-}EVI}$, $T_{opt\text{-}b\text{-}EVI}$); 3) compare the differences between EVI-based $T_{opt\text{-}sy}$ ($\mathbf{T_{opt-sy-EVI}}$) and GPP_{EC}-based $T_{opt\text{-}sy}$ ($\mathbf{T_{opt-sy-EC}}$); and 4) incorporate $\mathbf{T_{opt-sy-EVI}}$ and $\mathbf{T_{opt-b}}$ into the Vegetation Photosynthesis Model (VPM) (Xiao et al., 2004) to assess the differences in GPP_{VPM} estimates with $\mathbf{T_{opt-sy-EVI}}$ and with $\mathbf{T_{opt-b}}$. We used data from 165 eddy covariance flux sites in the FLUXNET network. We used daily daytime mean air temperature (T_{DT}) from the EC flux tower sites to delineate the start date of the growing season (SOS) and the end date of the growing season (EOS) for the site. The data within the growing season (SOS, EOS) were used to analyse the GPP-temperature and EVI-temperature relationships.

2. Materials and Methods

2.1. Study sites

We selected 165 eddy flux tower sites in the FLUXNET network using the following criteria: 1) each site had at least one year of observation (Table S1); 2) the flux site was dominated by one biome type within a radius of ~1 km around the site; 3) the dominant biome covered more than ~2/3 area of the 500 m MODIS pixel in which flux site was located. We overlaid the boundary of the MODIS pixel with high-resolution satellite imagery to visually interpret the land cover within the MODIS pixel and around the EC sites using the tool available on our website: http://www.eomf.ou.edu/modis/visualization/gmap/. Here we show the screenshots from the website for two eddy flux tower sites, one showing a site that is appropriate for comparison to a MODIS gridcell (Fig. S1), and the other showing a site that is not appropriate for such a comparison (Fig. S2). Th

tower sites include 11 biomes and a number of sites: 18 croplands (CRO), 2 closed shrublands (CSH), 21 deciduous broadleaf Forest (DBF), 14 evergreen broadleaf forest (EBF), 42 evergreen needleleaf forest (ENF), 25 grasslands (GRA), 9 mixed forest (MF), 8 open shrublands (OSH), 7 savannas (SAV), 13 wetlands (WET), and 6 woody savannas (WSA). Note that we assumed the GPP_{EC} well represented GPP in the MODIS pixel where the flux tower was located and was not affected largely by information from outside of the 1-km buffer. In fact, the eddy flux tower footprints are variable across sites, and are affected by factors such as wind speed, wind direction, tower height, and canopy type. Thus, tower footprints are very complicated and challenging to accurately estimate (Running et al., 1999; Waring et al., 1995). The 500-m square grid cell do not exactly overlay an EC tower footprint.

2.2. Climate and GPP data from the eddy flux tower sites

Meteorological data include incoming solar shortwave radiation (SW_IN_F) and daytime air temperature T_{DT}, which were input data in the VPM model. We used daily meteorological and GPP data in the FLUXNET-2015 dataset (http://fluxnet.fluxdata.org/data/fluxnet2015-dataset/). We used GPP_DT_VUT_REF, which was GPP estimated from observed net ecosystem exchange (NEE) data with the variable USTAR filtering approach and daytime partitioning method (Papale et al., 2006; Reichstein et al., 2005). We averaged the daily meteorological and GPP_{EC} data to 8-day temporal resolution such that it was consistent with the 8-day MODIS data.

2.3. MODIS land surface reflectance and vegetation indices for the eddy flux tower sites

We used MODIS spectral reflectance products MOD09A1 V006 with 500-m spatial resolution and 8-day temporal resolution. We calculated EVI, land surface water index (LSWI) Chandrasekar et al., 2010; Zhang et al., 2017), and Normalized Difference Snow Index (NDSI) with MOD09A1 V006 spectral bands using equations (1), ((2), and (3). MODIS bands are: red band (RED) (620–670 nm), near infrared band (NIR) (841–876 nm), blue band (BLUE) (459–479 nm), green band (GREEN) (545–565 nm), and short wavelength near infrared band (SWIR) (1628–1652 nm).

$$\mathbf{EVI} = \mathbf{2.5} \times \frac{\mathbf{NIR}-\mathbf{RED}}{(\mathbf{NIR}+\mathbf{6}\times\mathbf{RED}-\mathbf{7.5}\times\mathbf{BLUE}+\mathbf{1})} \quad (1)$$

$$\mathbf{LSWI} = \frac{\mathbf{NIR}-\mathbf{SWIR}}{\mathbf{NIR}+\mathbf{SWIR}} \quad (2)$$

$$\mathbf{NDSI} = \frac{\mathbf{GREEN}-\mathbf{SWIR}}{\mathbf{GREEN}+\mathbf{SWIR}} \quad (3)$$

Vegetation indices can be affected by clouds, cloud shadows, and soil background, so pre-processing of the time-series datasets are needed. We used data quality control (QC) layer for the identification of ice, snow, and cloud, and then gap-filled the affected observations with multi-year mean observation values Chang et al., 2019). We also used the Best Index Slope Extraction (BISE) method to identify abnormal observations missed by QC (Xiao et al., 2009). We used the Savitzky-Golay (S-G) method and smoothed the time-series data curves (Chang et al., 2019). We used EVI to estimate the fraction of photosynthetically active radiation absorbed by chlorophyll ($FPAR_{chl}$), and used LSWI to estimate the water scalar for the VPM model (Zhang et al., 2017), see equation (7) and ((9) respectively. We also used EVI to calculate $\mathbf{T_{opt-sy-EVI}}$ and $T_{opt\text{-}s\text{-}EVI}$.

2.4. MODIS land cover classification product

We used the MODIS MCD12Q1 v006 land cover data product. The studied 11 plant biomes, which have been decided from flux tower sites above, were classified using the Annual International Geosphere-Biosphere Programme (IGBP) classification system. We used land cover data for 2010 and calculated the area of each biome. Based on the area and GPP estimates, we then calculated annual total GPP for each biome.

2.5. Methods to estimate growing season from air temperature data at the sites

Snow affects MODIS EVI values at high-latitude, and EVI values at snow-covered sites were relatively high during winter. Here, we selected CA-SF1 (ENF) as an example, which is located in Canada. The site has a mean annual temperature 0.4°C. MODIS NDSI values are higher than 0.4 during winter, which indicates the presence of snow cover during this period (Fig. 1) (Chang et al., 2019). Due to snow, winter EVI values were higher than the highest summer EVI value at CA-SF1 (Fig. 1b). As temperature increases and snow melts, high winter EVI values decrease to its annual minimum, and then increase during spring or early summer because of leaf growth. NDSI decreases when T_{DT} reaches about 5°C. To reduce the effects from snow, global $T_{opt\text{-}sy}$ estimates from EVI should be based on data from the growing season, which is also snow-free peri

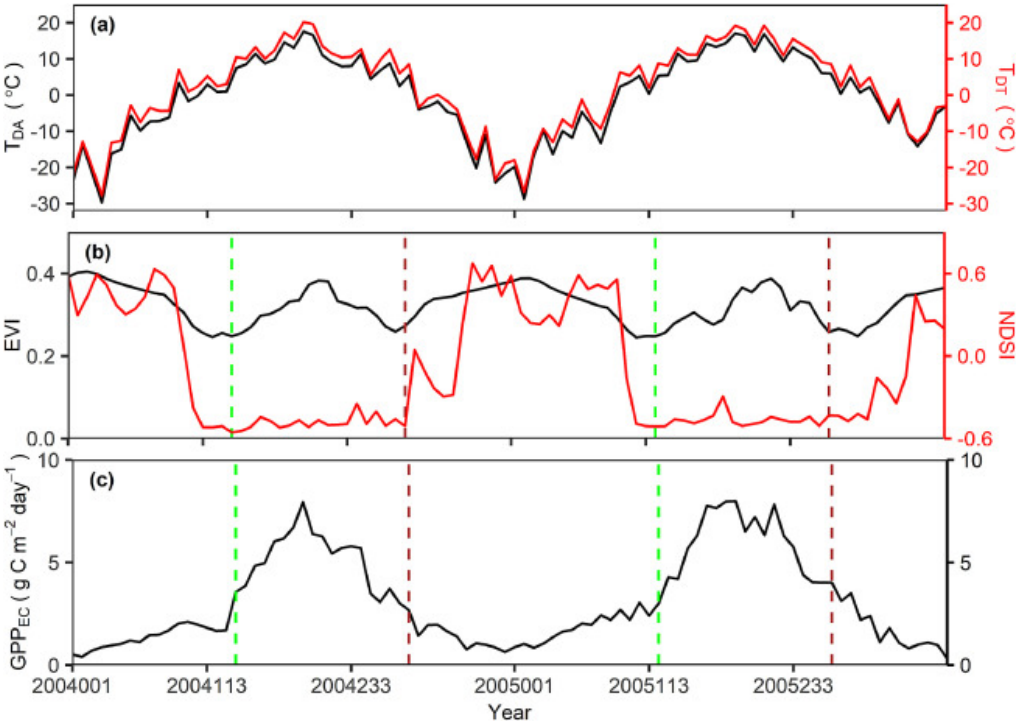

Download : Download high-res image (681KB) Download : Download full-size image

Fig. 1. Temporal dynamics of daily mean air temperature (T_{DA}), daily daytime mean air temperature (T_{DT}), MODIS NDSI, MODIS EVI, and GPPEC during 2004-2005 at the CA-SF1 flux site. This site is evergreen needleleaf forest (ENF). EVI values during winter at this site are affected by snow cover. Vertical green dashed lines represent the start of the snow-free growing season (SOS) and vertical brown dashed lines are the end of snow-free growing season (EOS).

We used T_{DT} and the degree-day accumulated temperature model to determine the start of the snow-free growing season (SOS) and the end of the snow-free growing season (EOS), and to assess the snow-free period for each year. The degree-day model assumes that the minimum temperature for plant growth is 5°C (Chang et al., 2019; Prentice et al., 1992). The SOS date was defined as the date when T_{DT} was above 5°C and would last for at least three 8-day observations (Chang et al., 2019), and the EOS date was defined as the date when T_{DT} was lower than 5°C at the next observation (Fig. 1). We estimated SOS and EOS for each site-year at the 165 flux sites, and the multi-year mean SOS and EOS for individual sites were shown in Fig. S3.

2.6. Methods to estimate site-year-specific and site-specific optimum air temperature of photosynthesis from GPP_{EC} and EVI data

We estimated $\mathbf{T_{opt-sy}}$ values for each site-year from both GPP_{EC} and MODIS EVI. $\mathbf{T_{opt-sy}}$ values were defined as the average air temperature of the observations with GPP_{EC} (or EVI) equal or higher than 95% of the maximum GPP_{EC} (or EVI) during the growing season. Site-specific optimum air temperature ($\mathbf{T_{opt-s}}$) was calculated as multi-year mean $\mathbf{T_{opt-sy}}$ for each site. We estimated $\mathbf{T_{opt-sy}}$ and $\mathbf{T_{opt-s}}$ using both 8-day T_{DT} and 8-day daily mean air temperature (T_{DA}). As T_{DA} includes both daytime and night-time temperature, there are notable differences between T_{DT} and T_{DA} (Fig. S4). The T_{opt-s} calculated from T_{DT} and T_{DA} have 2°C difference (Fig. S5). As we intended to analyze the photosynthesis-temperature relationship, we used T_{DT} which is more appropriate than T_{DA} for T_{opt} calculation and GPP simulation.

2.7. Methods to assess the effect of biome-specific and site-year-specific optimum air temperature on GPP estimates

VPM is a satellite-based LUE model that estimates 8-day GPP using absorbed photosynthetically active radiation by chlorophyll ($APAR_{chl}$) and light use efficiency (ε) Xiao et al., 2004). The VPM equations are listed as equation (4) to ((9). In these equations, ε is light use efficiency, $\mathbf{APAR_{chl}}$ is the absorbed photosynthetically active radiation by chlorophyll, $\mathbf{PAR}$ is the amou

photosynthetic active radiation at the top of the canopy, $\mathbf{FPAR_{chl}}$ is the fraction of PAR absorbed by chlorophyll, which is calculated from EVI using linear regression. $\mathbf{FPAR_{chl}}$ calculated from EVI was suggested to be more appropriate to represent pigment-level energy process, which is directly correlated to GPP, than the canopy-level FPAR products (Zhang et al., 2013; Zhang et al., 2009). Previous publications suggested that using $FPAR_{chl}$ from EVI can better capture the seasonal variation of vegetation photosynthetic capacity and greatly improve the models that estimate GPP than using MODIS canopy-level FPAR product (MOD15A2H) (Zhang et al., 2014; Zhang et al., 2017). ε is downscaled from the maximum light used efficiency (ε_0) with temperature ($\mathbf{T_s}$) and water scalars ($\mathbf{W_s}$). $\mathbf{T_s}$ is calculated as a function of minimum temperature ($\mathbf{T_{min}}$), maximum temperature ($\mathbf{T_{max}}$), and optimum temperature for plant growth ($\mathbf{T_{opt}}$). $\mathbf{W_s}$ is calculated as a function of LSWI and the maximum LSWI in a 5-years moving window during the growing season.

$$\mathbf{GPP_{VPM}} = \varepsilon \times \mathbf{APAR_{chl}} \tag{4}$$

$$\mathbf{APAR_{chl}} = \mathbf{FPAR_{chl}} \times \mathbf{PAR} \tag{5}$$

$$\varepsilon = \varepsilon_0 \times \mathbf{T_s} \times \mathbf{W_s} \tag{6}$$

$$\mathbf{FPAR_{chl}} = 1.25 \times (\mathbf{EVI} - 0.1) \tag{7}$$

$$\mathbf{T_s} = \frac{(T_{DT} - T_{min})(T_{DT} - T_{max})}{(T_{DT} - T_{min})(T_{DT} - T_{max}) - (T_{DT} - T_{opt})^2} \tag{8}$$

$$\mathbf{W_s} = \frac{(1+LSWI)}{(1+LSWI_{max})} \tag{9}$$

We incorporated $T_{opt\text{-}b}$ and $T_{opt\text{-}sy}$ into the Vegetation Photosynthesis Model (VPM) and compared GPP_{VPM} calculated from both parameters with GPP_{EC} to determine which temperature parameter performed best. $\mathbf{T_{opt-b-LT}}$ followed the setting in global VPM GPP product (Zhang et al., 2017), see the marked orange stars in Fig. 4.

3. Results

3.1. Estimates of biome-specific optimum air temperature from GPP_{EC} and EVI

The response curves of both GPP_{EC} and EVI to T_{DT} were similar and show typical bell-shaped photosynthesis-temperature relationships (Fig. 2). T_{DT} at peak EVI was close to T_{DT} at peak GPP_{EC} across the biome types. In addition, our regression analysis showed that the $\mathbf{T_{opt-b-EC}}$ values differed to the $\mathbf{T_{opt-b-LT}}$ used in the global VPM product ($\mathbf{T_{opt-b-LT}}$ values are marked as orange stars in Fig. 4). Specifically, $\mathbf{T_{opt-b-LT}}$ were higher than $\mathbf{T_{opt-b}}$ estimated from EVI ($\mathbf{T_{opt-b-EVI}}$) and $\mathbf{T_{opt-b}}$ from GPP_{EC} ($\mathbf{T_{opt-b-EC}}$) in CRO, EBF, GRA, OSH, and SAV biomes. Differences between $\mathbf{T_{opt-b-LT}}$ and $\mathbf{T_{opt-b-EC}}$ in OSH and GRA were 14.03 °C and 9.31°C respectively, which were much higher than the differences in other biomes (Table. S2). $\mathbf{T_{opt-b-LT}}$ values were lower than $\mathbf{T_{opt-b-EC}}$ in CSH, DBF, MF, WET, and WSA biomes by 1.00 °C to 5.55 °C.

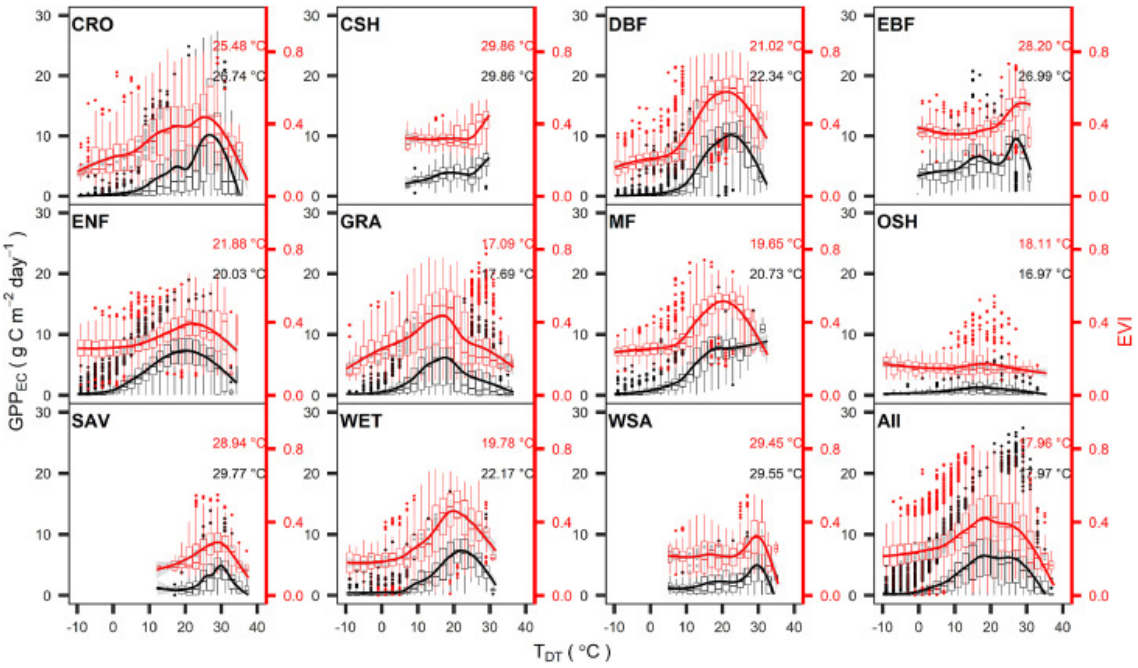

Download : Download high-res image (1MB) Download : Download full-size image

Fig. 2. The relationships between GPP estimates (GPP_{EC}) from the flux tower data and EVI and daily daytime mean air temperature (T_{DT}) within individual biomes. Solid black and red lines are fitting curves for GPP_{EC} and EVI using a cyclic penalized cubic regression spline. Annotated text numbers in each panel represent the daily daytime mean air temperature when GPP_{EC} (black) or EVI (red) peak in a year. As there are large amount of observation points, we showed boxplots for points in 2 degree C bins in panels.

3.2. Estimates of site-year-specific and site-specific optimum air temperature from GPP_{EC} and EVI

The linear regression analysis indicated that $\mathbf{T_{opt-sy-EVI}}$ was significantly correlated with $\mathbf{T_{opt-sy-EC}}$ ($P < 0.001$) (Fig. 3). The difference between $\mathbf{T_{opt-sy-EVI}}$ and $\mathbf{T_{opt-sy-GPP_{EC}}}$ ranged from 2 °C in WSA to 4.85°C in CSH. $\mathbf{T_{opt-sy}}$ showed large variations across sites and years within individual biomes. The dynamic ranges from minimum to maximum $\mathbf{T_{opt-sy}}$ among site-years within a biome differed across biomes (Fig. 4). Specifically, the dynamic range of $\mathbf{T_{opt-sy-EC}}$ was lowest in SAV with 8.13°C and highest in ENF with 23.52 °C. On average, the dynamic ranges of $\mathbf{T_{opt-sy-EC}}$ and $\mathbf{T_{opt-sy-EVI}}$ for the selected 11 biomes were 17.25 °C and 18.85 °C, respectively. Both $\mathbf{T_{opt-sy-EC}}$ and $\mathbf{T_{opt-sy-EVI}}$ had a higher dynamic range within ENF and GRA (> 20°C) than other biomes, and the lowest dynamic range in SAV (Fig. 4, Fig. S6).

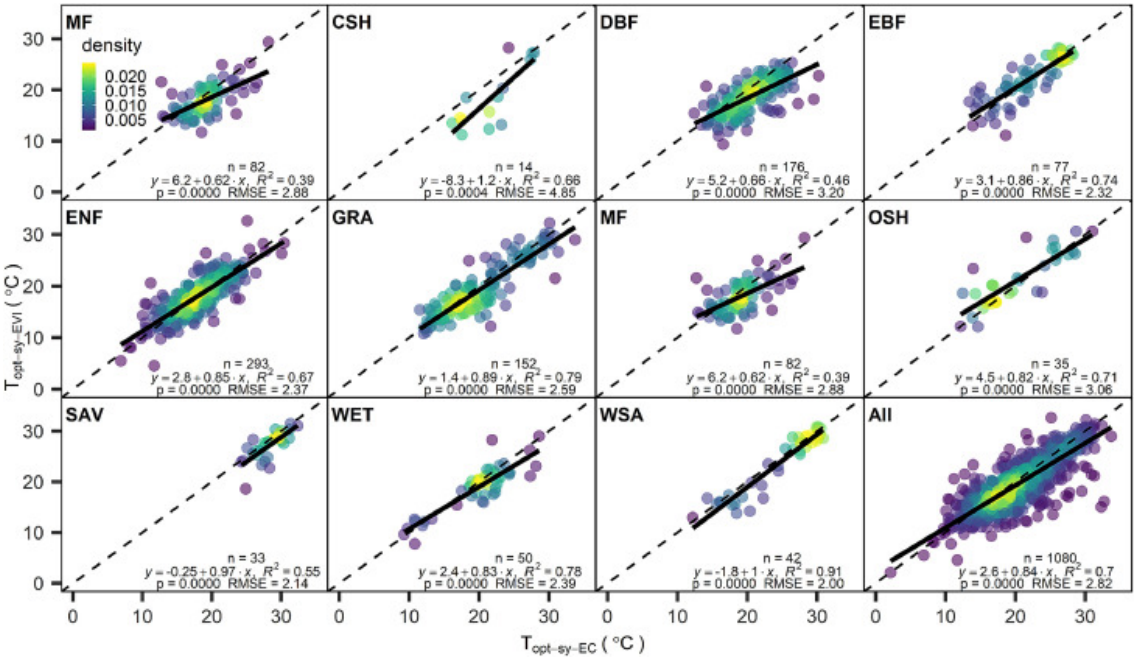

Download : Download high-res image (1MB) Download : Download full-size image

Fig. 3. Relationships between site-year-specific optimum air temperature ($\mathbf{T_{opt-sy}}$) estimated from EVI ($\mathbf{T_{opt-sy-EVI}}$) and $\mathbf{T_{opt-sy}}$ from GPP_{EC} ($\mathbf{T_{opt-sy-EC}}$) across the biomes. "n" represents the number of site-years for each biome.

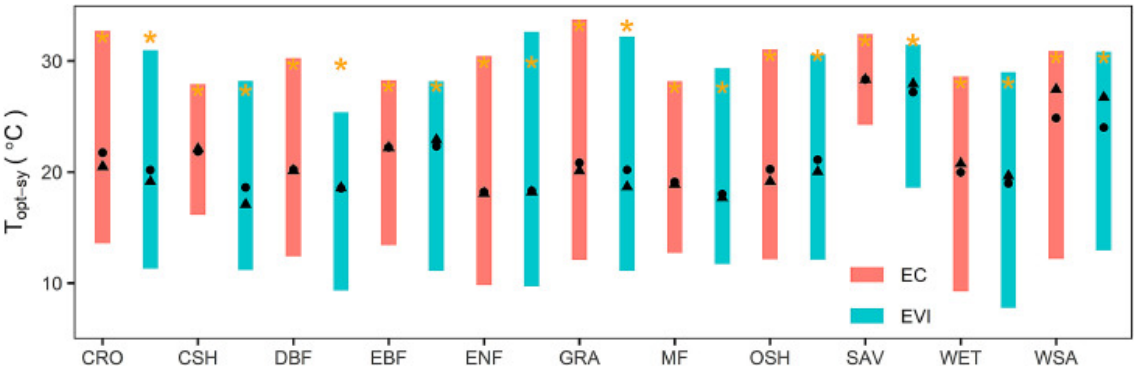

Download : Download high-res image (307KB) Download : Download full-size image

Fig. 4. Site-year-specific optimum air temperature ($\mathbf{T_{opt-sy}}$) values estimated from GPP_{EC} ($\mathbf{T_{opt-sy-EC}}$, red bars) and EVI ($\mathbf{T_{opt-sy-EVI}}$, blue bars) for different biomes. For a given biome, the bar bottom represents the minimum value for all the sites, bar top is maximum value, black dot is mean value, black triangle is median value, orange star is optimum air temperature suggested in look up table ($\mathbf{T_{opt-b-LT}}$).

The site-year specific optimum air temperature ($\mathbf{T_{opt-sy}}$) was different than the $\mathbf{T_{opt-b-LT}}$ values (Fig. 4). $\mathbf{T_{opt-b-LT}}$ for CRO was 30 °C while $\mathbf{T_{opt-sy-EC}}$ ranged from 13.59 °C to 32.70 °C and was 21.74 °C on average. Most of the mean $\mathbf{T_{opt-sy-EC}}$ and $\mathbf{T_{opt-sy-EVI}}$ values were substantially lower than $\mathbf{T_{opt-b-LT}}$ across biomes, especially in CRO, EBF, GRA, and OSH. Compared with mean $\mathbf{T_{opt-sy-EC}}$, the $\mathbf{T_{opt-b-LT}}$ of CRO, EBF, GRA, and OSH in the global VPM were higher by ~8 °C, 6 °C, 7 °C, and 11 °C, respectively.

The site-specific optimum temperature ($\mathbf{T_{opt-s}}$) values from MODIS EVI ($\mathbf{T_{opt-s-EVI}}$) were also significantly correlated to $\mathbf{T_{opt-s}}$ from GPP_{EC} ($\mathbf{T_{opt-s-EC}}$) ($P < 0.001$) with a RMSE of 1.99 °C (Fig. 5 a). $\mathbf{T_{opt-s}}$ values ranged from ~10 °C to ~30 °C across the 165 flux tower sites (Fig. S7). Both $\mathbf{T_{opt-s-EC}}$ and $\mathbf{T_{opt-s-EVI}}$ were highly variable among sites within a biome (Fig. 5 b,c). The highest dynamic range of $\mathbf{T_{opt-s}}$ was in GRA. The difference between the higher and lower quartiles in GRA was as high as ~10°C. $\mathbf{T_{opt-s-EC}}$ and $\mathbf{T_{opt-s-EVI}}$ also varied significantly across CRO, EBF, CSH, and WSA sites. In addition, there was a strong linear relationship between $\mathbf{T_{opt-s}}$ and annual T_{DT} ($P < 0.001$, $R^2 = 0.61$) (Fig. 5 a). Also, there were strong longitudinal gradients of $\mathbf{T_{opt-s}}$ for the flux sites (Fig. 6). Specifically, we found no clear latitudinal change in $\mathbf{T_{opt-s}}$ in the tropical region (an average ~27 °C), while $\mathbf{T_{opt-s}}$ sharply decreased from low to high latitudes.

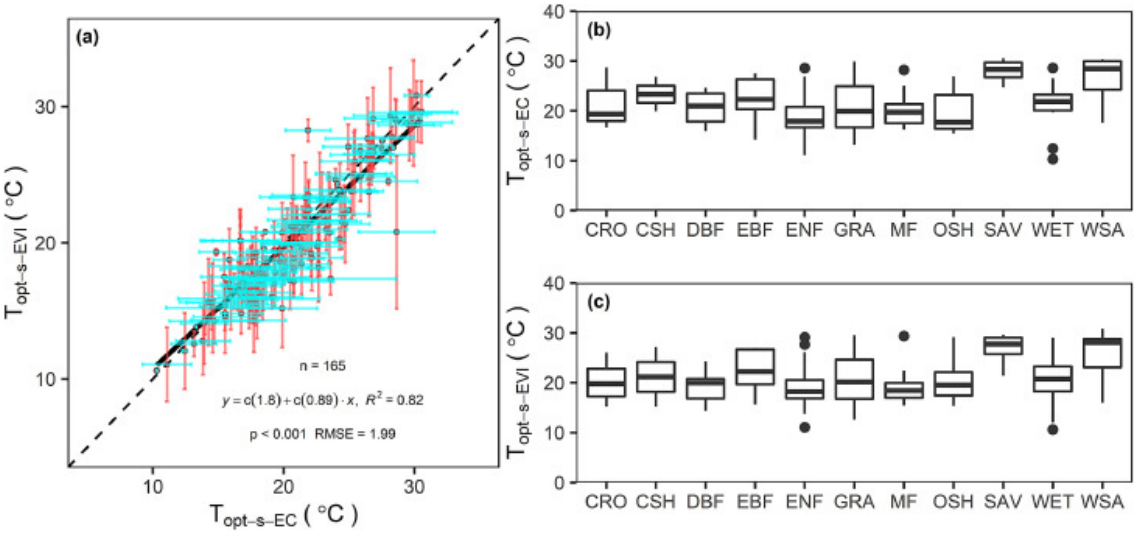

Download : Download high-res image (571KB) Download : Download full-size image

Fig. 5. Relationships and distribution of site-specific optimum air temperature ($\mathbf{T_{opt-s}}$) estimated from GPP_{EC} ($\mathbf{T_{opt-s-EC}}$) and EVI ($\mathbf{T_{opt-s-EVI}}$). (a) Linear regression of $\mathbf{T_{opt-s-EVI}}$ and $\mathbf{T_{opt-s-EC}}$ for the 165 flux tower sites. (b) Boxplot of $\mathbf{T_{opt-s-EC}}$ for different biomes. (c) Boxplot of $\mathbf{T_{opt-s-EVI}}$ for different biomes. $\mathbf{T_{opt-s}}$ was defined as the multi-year mean value of $\mathbf{T_{opt-sy}}$ for each site.

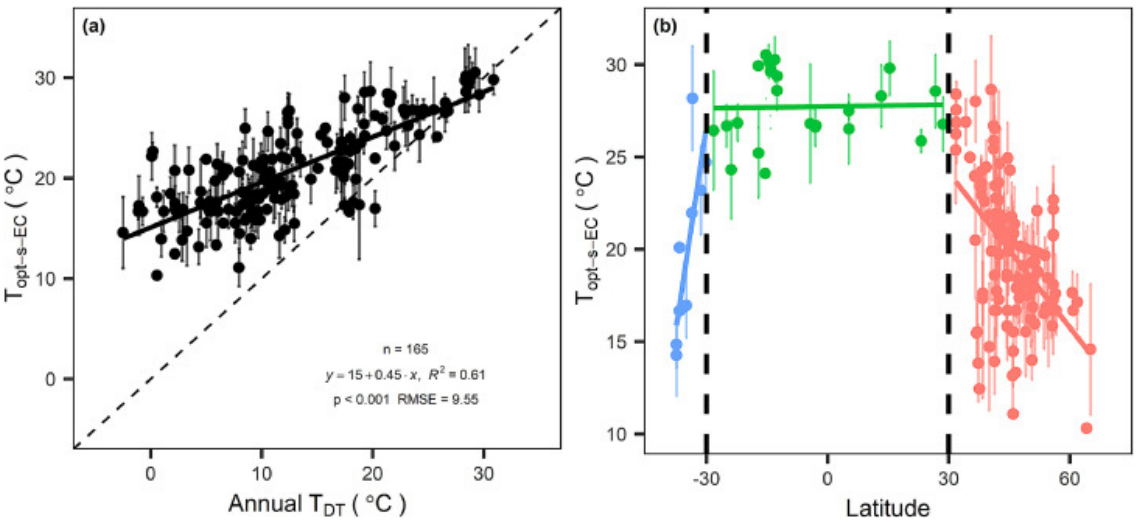

Download : Download high-res image (500KB) Download : Download full-size image

Fig. 6. Relationship of site-specific temperature from flux tower GPP_{EC} ($\mathbf{T_{opt-s-GPP_{EC}}}$) to (a) annual mean daytime air temperature and (b) latitude.

3.3. The effects of biome-specific and site-year-specific optimum air temperature on GPP estimates

GPP_{VPM} simulated with $\mathbf{T_{opt-sy-EVI}}$ ($\mathbf{GPP_{VPM-sy-EVI}}$) were significantly correlated with 8-day GPP_{EC} across all the studied biomes ($p < 0.001$) (Fig. 7). Compared with GPP_{VPM} simulated with $\mathbf{T_{opt-b-LT}}$ ($\mathbf{GPP_{VPM-b-LT}}$), $\mathbf{GPP_{VPM-sy-EVI}}$ had a lower RMSE value for most biomes than $\mathbf{GPP_{VPM-b-LT}}$ when compared to GPP_{EC}. The 8-day $\mathbf{GPP_{VPM-b-LT}}$ values were much lower than GPP_{EC} observations during summer season when GPP is high, especially for CRO, ENF, EBF, GRA, SAV, and WSA. $\mathbf{GPP_{VPM-sy-EVI}}$ were higher than $\mathbf{GPP_{VPM-b-LT}}$, especially for CRO and GRA. For all the biomes, the linear regression slopes of $\mathbf{GPP_{VPM-sy-EVI}}$ versus GPP_{EC} were much closer to one than $\mathbf{GPP_{VPM-b-LT}}$ versus GPP_{EC}.

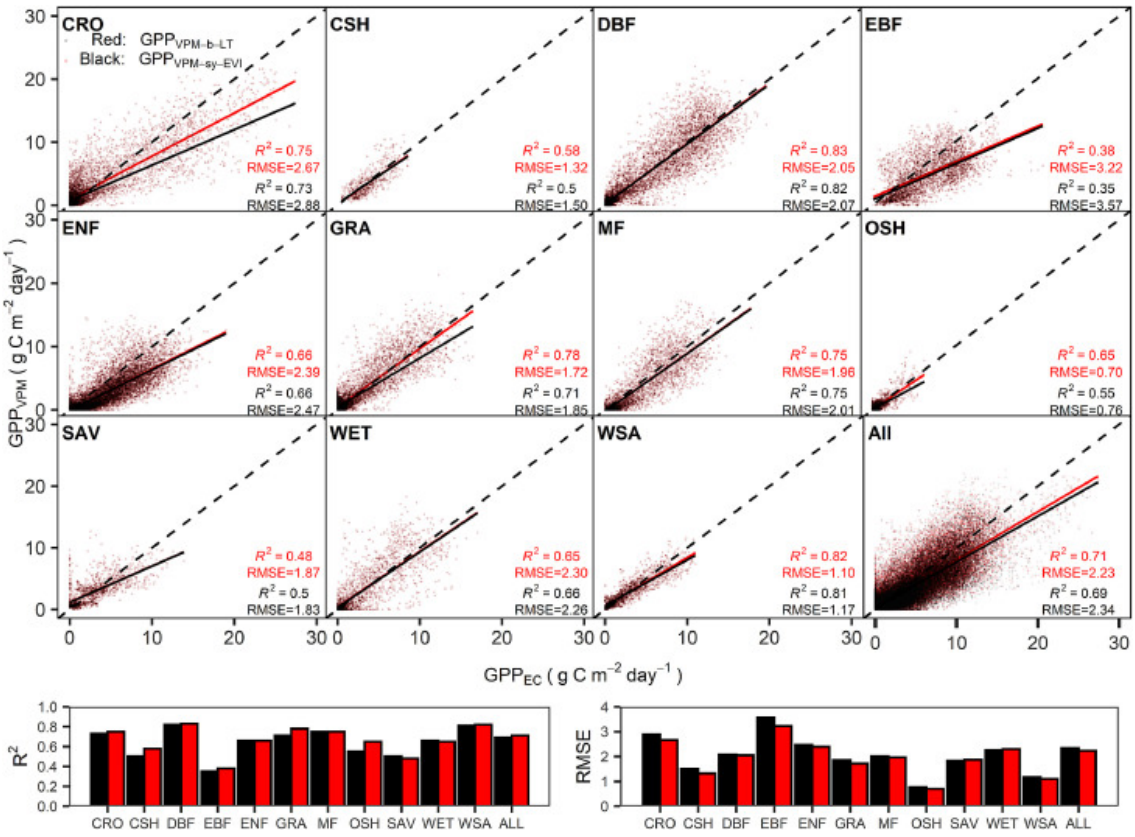

Download : Download high-res image (1MB) Download : Download full-size image

Fig. 7. A comparison of daily GPP estimates (g C/m^2/day) from VPM simulation with $\mathbf{T_{opt-sy-EVI}}$ ($\mathbf{GPP_{VPM-sy-EVI}}$), VPM simulation with $\mathbf{T_{opt-b-LT}}$ ($\mathbf{GPP_{VPM-b-LT}}$), and eddy covariance flux tower GPP (GPP_{EC}) in 8-day interval.

Annual $\mathbf{GPP_{VPM-sy-EVI}}$ was also significantly correlated with GPP_{EC} across the biomes (Fig. 8). The linear regression analysis between $\mathbf{GPP_{VPM-sy-EVI}}$ and GPP_{EC} showed higher R^2 values and lower RMSE values than that between $\mathbf{GPP_{vpm-b-LT}}$ and GPP_{EC}. Multi-year average annual GPP estimated by $\mathbf{GPP_{VPM-b-LT}}$ underestimated GPP for all the biomes by varying amounts (Table 1). Annual $\mathbf{GPP_{VPM-sy-EVI}}$ estimates were higher than $\mathbf{GPP_{VPM-b-LT}}$ for all biomes except CSH and were closer to GPP_{EC}. For instance, annual $\mathbf{GPP_{VPM-sy-EVI}}$ was higher than $\mathbf{GPP_{VPM-b-LT}}$ by more than 100 g C m^{-2} yr^{-1} in CRO (186 g C m^{-2} yr^{-1}), EBF (145 g C m^{-2} yr^{-1}), and GRA (184 g C m^{-2} yr^{-1}). Annual $\mathbf{GPP_{VPM-sy-EVI}}$ was higher than $\mathbf{GPP_{VPM-b-LT}}$ with varying ratios across biomes, which ranged from 1% to 34%. Specifically, Annual $\mathbf{GPP_{VPM-sy-EVI}}$ was higher than $\mathbf{GPP_{VPM-b-LT}}$ by 34% for OSH, 18% for CRO, and 19% for GRA. Annual $\mathbf{GPP_{VPM-b-LT}}$ in OSH was 224 g C m^{-2} yr^{-1} while annual $\mathbf{GPP_{VPM-sy-EVI}}$ was 301 g C m^{-2} yr^{-1}, which was much higher. In a simple calculation for illustrative purposes, at the global scale $\mathbf{GPP_{VPM-b-LT}}$ was ~10 Pg C/yr lower than $\mathbf{GPP_{VPM-sy-EVI}}$ (Table 1). These results clearly show that replacing the static and biome-specific $\mathbf{T_{opt-b-LT}}$ values with site- and site-year specific values, such as $\mathbf{T_{opt-sy-EVI}}$, can have a large impact on GPP estimates at global scale.

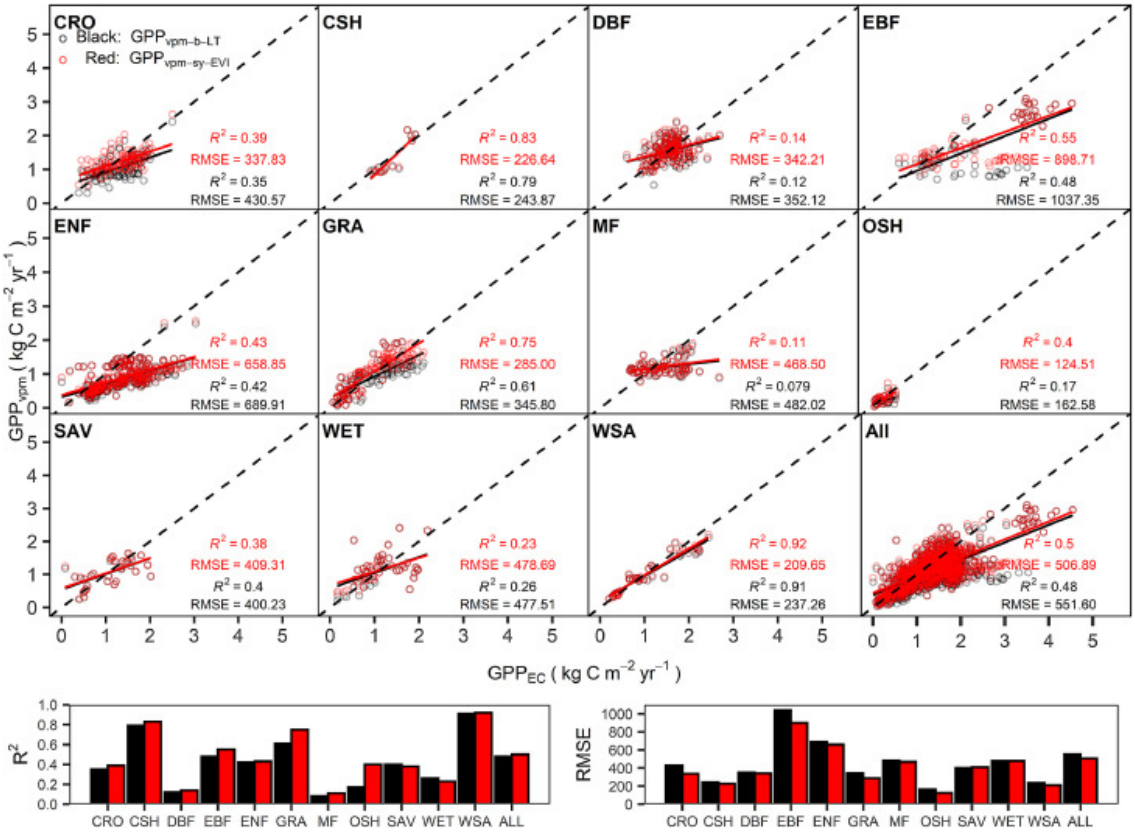

Download : Download high-res image (1MB) Download : Download full-size image

Fig. 8. A comparison of annual GPP_{VPM} (kg C/m^2/yr) simulated with $\mathbf{T_{opt-sy-EVI}}$ ($\mathbf{GPP_{VPM-sy-EVI}}$) and annual GPP_{VPM} with $\mathbf{T_{opt-b-LT}}$ ($\mathbf{GPP_{VPM-b-LT}}$) against annual GPP from eddy covariance flux sites (GPP_{EC}) across biome types (biomes).

Table 1. Annual GPP (g C m^{-2} yr^{-1}) comparison among GPP_{EC}, $\mathbf{GPP_{VPM-b-LT}}$, and $\mathbf{GPP_{VPM-sy-EVI}}$ at the biome and global scales. Note that these numbers are a simple calculation with 11 of all the biome types and used only for illustrating the likely differences, and they are much lower than the numbers from VPM global simulations at individual pixels (Zhang et al., 2017).

Biome Type	Annual Mean (g C/m^2/yr)			Difference		Biome area (10^7 km^2)	Annual Total (Pg C/yr)	
	GPP_{EC}	$GPP_{VPM-b-LT}$	$GPP_{VPM-sy-EVI}$	GPP (g /m^2/yr)	Ratio		$GPP_{VPM-b-LT}$	$GPP_{VPM-sy-EVI}$
CRO	1308.08	1048.86	1234.83	185.96	17.73%	1.01	10.60	12.48
CSH	1358.83	1282.76	1234.59	-48.17	-3.76%	0.03	0.42	0.41
DBF	1567.88	1543.76	1572.00	28.23	1.83%	0.23	3.53	3.59
EBF	2412.94	1662.70	1807.88	145.18	8.73%	0.82	13.56	14.74
ENF	1372.88	846.79	883.74	36.95	4.36%	0.27	2.28	2.38
GRA	1191.89	988.57	1172.73	184.15	18.63%	2.71	26.79	31.78
MF	1414.49	1205.11	1216.54	11.42	0.95%	0.49	5.95	6.01
OSH	307.43	224.36	301.19	76.83	34.25%	1.41	3.16	4.24

Biome Type	Annual Mean (g C/m^2/yr)			Difference		Biome area (10^7 km^2)	Annual Total (Pg C/yr)	
	GPP_{EC}	$GPP_{VPM-b-LT}$	$GPP_{VPM-sy-EVI}$	GPP (g /m^2/yr)	Ratio		$GPP_{VPM-b-LT}$	$GPP_{VPM-sy-EVI}$
SAV	1078.44	1053.15	1066.70	13.55	1.29%	1.43	15.11	15.30
WET	1093.06	1091.54	1124.37	32.84	3.01%	0.10	1.08	1.11
WSA	1103.08	1033.81	1063.38	29.57	2.86%	1.08	11.20	11.52
Annual Total GPP for Selected Biomes							93.68	103.57

Difference of annual GPP is calculated as ($GPP_{VPM-sy-EVI}$ - $GPP_{VPM-b-LT}$). Improvement of ratio is calculated as ($GPP_{VPM-sy-EVI}$ - $GPP_{VPM-b-LT}$) / $GPP_{VPM-b-LT}$. Annual total GPP is calculated as (annual mean GPP × biome area).

We also compared the GPP estimates using $T_{opt-b-LT}$ and $T_{opt-b-EC}$. We selected 5 biomes in which differences between $T_{opt-b-LT}$ and $T_{opt-b-EC}$ were larger than 3 °C: CRO (3.2 °C), CSH (4. 8°C), GRA (9.31 °C), OSH (14.03 °C), and WSA (5.55 °C) (Fig. 2, Table S2). Then we simulated GPP_{VPM} for the 5 biomes using the two forms of T_{opt-b}. We found that GPP_{VPM} estimates were significantly improved relative to GPP_{EC} when using $T_{opt-b-EC}$ rather than $T_{opt-b-LT}$ across the 5 biomes at both the 8-day and annual time scale (Fig. 9).

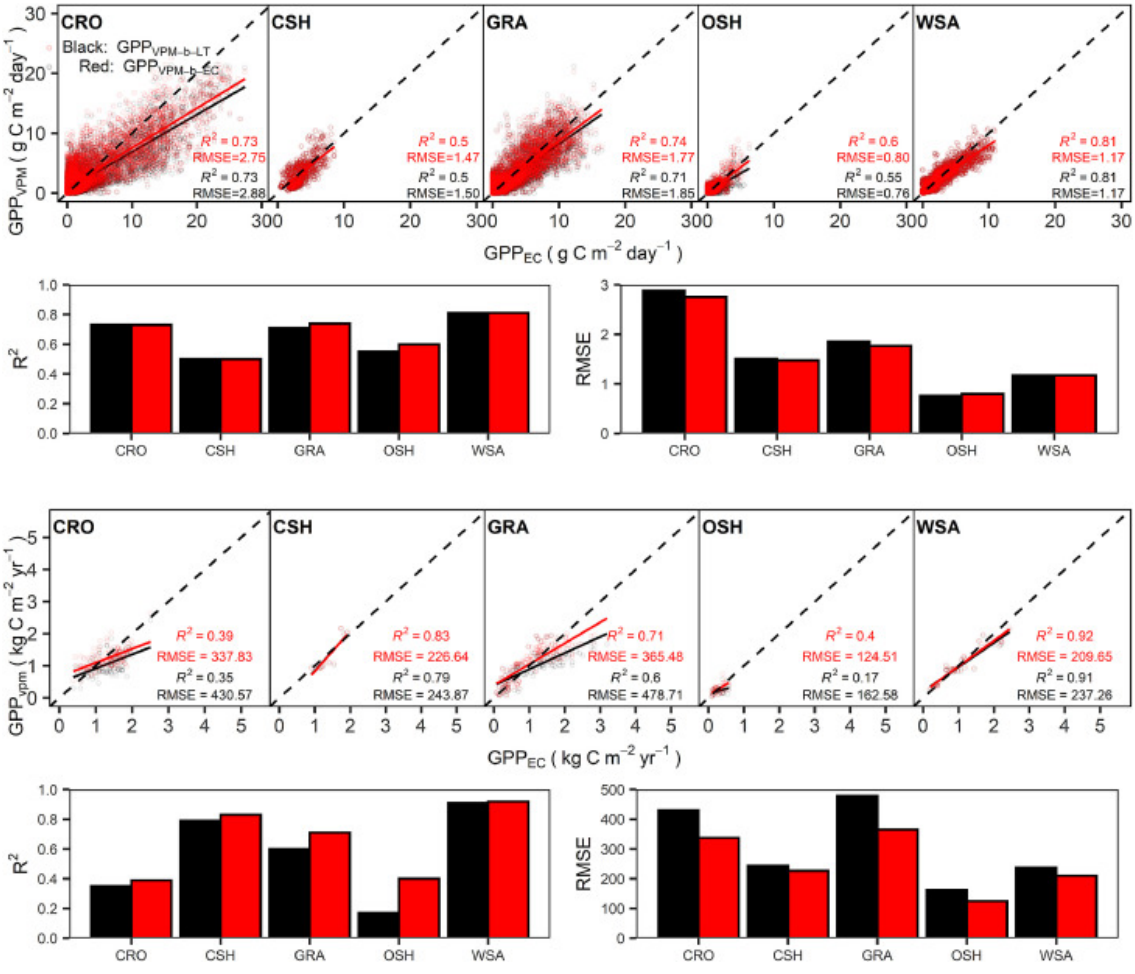

Download : Download high-res image (1MB) Download : Download full-size image

Fig. 9. Comparisons of GPP_{VPM} simulated with $T_{opt-b-LT}$ ($GPP_{VPM-b-LT}$) and GPP_{VPM} simulated with $T_{opt-b-EC}$ ($GPP_{VPM-b-EC}$) against eddy covariance flux tower GPP (GPP_{EC}) for CRO, CSH, GRA, OSH and WSA in 8-day intervals (top row) and annually (bottom row).

FEEDBACK

4. Discussion

4.1. The limitation of biome-specific optimum air temperature

The $\mathbf{T_{opt-b}}$ values based on GPP_{EC} and T_{DT} in our study differed greatly relative to the $\mathbf{T_{opt-b-LT}}$ used in previous global GPP models across biomes (Fig. 2, Table S2). Biome-specific maximum, minimum, and optimum temperature parameters in most of the global GPP models, such as VPM, TEM (Melillo et al., 1993; Raich et al., 1991), TEC (Yan et al., 2015), and EC-LUE (Yuan et al., 2007), use the look-up table generated by the TEM model (Melillo et al., 1993). As presented, the biome-specific parameters in this look-up table were taken from two papers: McGuire et al. (1992) and Raich et al. (1991). However, in both publications a limited number of sites and a few biomes were used to determine the parameters. Specifically, Raich et al. (1991) defined biome-specific parameters from only 12 sites with 7 biomes in South America. McGuire et al. (1992) defined biome-specific parameters based on 16 sites with 16 biomes. Note that 10 of the 16 sites were in the United States while the others were in Canada, New Zealand, South Africa, Puerto Rico, India, and Brazil. The limited number of sites and biomes used to determine biome-specific parameters introduces large uncertainties. In addition, biome-specific temperature parameters in Raich et al. (1991) and McGuire et al. (1992) were defined using information from Larcher (1980), which was mostly based on field and laboratory studies at the leaf or plant scales rather than the canopy. Therefore, uncertainty is introduced when parameters from the look-up table are used to estimate GPP.

The results from our analysis of GPP_{EC}, EVI, and TemDT provides guidance for future studies on the relationship between photosynthesis and air temperature and for determining optimal temperature parameters for terrestrial biochemical models. We generated $\mathbf{T_{opt-b-EC}}$ parameters using 165 flux tower sites across 11biomes. The number of flux towers sites used for determining $\mathbf{T_{opt-b}}$ in our study is much larger than in previous studies and is more applicable for global applications. Global GPP model estimates derived using $\mathbf{T_{opt-b-LT}}$ introduces uncertainty in the estimates. From the LUE model, one can conclude that the higher values of $\mathbf{T_{opt-b-LT}}$ than $\mathbf{T_{opt-b-EC}}$ will result in the underestimation of GPP in CRO, EBF, GRA, OSH, and SAV. Replacing $\mathbf{T_{opt-b-LT}}$ with $\mathbf{T_{opt-b-EC}}$ in GPP simulations can improve GPP estimates. The biome-specific look-up table can be updated using our $\mathbf{T_{opt-b-EC}}$ values, which is expected to improve GPP estimates.

4.2. The contribution of site-year-specific optimum air temperature to GPP estimates

The site-year-specific temperature parameters estimated in our study comprehensively considered the variations of temperature constraints among biomes, environmental conditions, and ecosystems. $\mathbf{T_{opt-sy}}$ varied considerably across sites and years, and largely differed to $\mathbf{T_{opt-b-LT}}$ and $\mathbf{T_{opt-b-EC}}$ (Fig. 4). The large difference between $\mathbf{T_{opt-sy}}$ and $\mathbf{T_{opt-b-LT}}$ indicated that biome-specific parameters should be adjusted in terrestrial biochemical models. Previous studies have suggested that static parameters in the biome-specific look-up table introduce uncertainty in GPP estimates but did not address how the biome-specific parameters, especially temperature, affect the accuracy of modelled-GPP products (Sjöström et al., 2013; Zhao and Running, 2010). We not only compared the differences between $\mathbf{T_{opt-sy}}$, $\mathbf{T_{opt-b-LT}}$, and $\mathbf{T_{opt-b-EC}}$, but also examined the differences of how they perform in estimating GPP across biomes.

Results of our study point to the potential development of a LUE-based GPP model based on $\mathbf{T_{opt-sy}}$. We demonstrated that GPP estimates in GRA, CRO, and OSH benefit most from $\mathbf{T_{opt-sy}}$. Because of their wide distribution across various geographical and ecological regions (Friedl et al., 2002), photosynthesis or growth of GRA, CRO, and OSH are particularly sensitive to temperature dynamics (Wang et al., 2018; Wu et al., 2018a). The $\mathbf{T_{opt-b-LT}}$ parameters used in the global GPP_{VPM} estimates are much higher than most of the $\mathbf{T_{opt-sy}}$ in these biomes. Using $\mathbf{T_{opt-b-LT}}$ in the global GPP_{VPM} product underestimated GPP for the selected 11 biomes by about 10 Pg C/yr (Table 1), which indicated that total global GPP could be ~130-140 Pg C/yr instead of ~120-130 Pg C/yr. Multi-year mean values of $\mathbf{T_{opt-sy}}$ calculated in our study were also much lower than $\mathbf{T_{opt-b-LT}}$ used in other GPP models for most biomes, such as in TEC (Yan et al., 2015) and EC-LUE (Yuan et al., 2007), which could also have led to underestimations of GPP by these models. In summary, using $\mathbf{T_{opt-sy}}$ is an efficient approach for improving future's regional and global GPP estimates.

The improved GPP product will can be used for the study of terrestrial carbon cycle. Based on global GPP product estimated by machine-learning technique using FLUXNET measurements, a study found that croplands have higher photosynthetic capacity than other vegetation types, and that croplands expansion moderately dominated the increase of peak global GP

in annual GPP (Huang et al., 2018). Improved GPP products may show that agricultural intensification could have stronger than anticipated impacts on vegetation productivity. Also, the grassland biome is the largest in the world and grassland productivity are highly sensitive to climate variability (Hovenden et al., 2014). Grassland productivity has been found to be increasing under warmer mean annual temperatures (Fridley et al., 2016; Hufkens et al., 2016). Considering the high underestimation of grassland GPP by models with biome-specific temperature parameters, grassland could actually have performed larger variability if we use GPP estimated using site-specific parameters.

4.3. Other sources of error and uncertainty in satellite-based GPP estimates

Even though we have incorporated $\mathbf{T_{opt-sy}}$ instead of $\mathbf{T_{opt-b-LT}}$ into GPP simulation and improved GPP estimates, $GPP_{VPM\text{-}sy\text{-}EVI}$ values are still lower than GPP_{EC} (Fig. 7, Fig. 8). One uncertainty could come from the inaccurate estimation of temperature parameters because of the limited number and poor distribution of flux tower sites. For example, there were only two CSH site available for our study and it was not possible to detect the peak from regression lines (Fig. 2). Underestimation is a common problem in many satellite-based GPP estimates, such as with the MODIS GPP product (Sjöström et al., 2013; Zhu et al., 2018). Many parameters other than $T_{opt\text{-}b}$ have been reported as sources of error and uncertainty in satellite-based GPP, such as model structure, forcing data, and parameter selection (Zheng et al., 2018).

For warmer and water-limited sites in southern Europe, water availability has been reported to be an important factor limiting GPP, while air temperature can better explain the variability of GPP at cold northern sites (Reichstein et al., 2007). Temperature was not a limiting factor or significant driver in some biomes, such as SAV and WSA (Ma et al., 2014), so adjusting temperature in our study could not significantly improve GPP estimate in these biomes. Some studies have pointed out that satellite-based GPP do not consider soil moisture, and thus fail to accurately estimate the magnitude of canopy GPP under drought or water deficit (Kanniah et al., 2009; Stocker et al., 2019). Even though VPM uses LSWI as a proxy for land surface water content, the model still failed accurately determining the information of soil moisture, which has been assumed to contribute more to explaining GPP variability than other water proxies like VPD (Ryu et al., 2019).

The quality and accuracy of input data can also introduce uncertainties into GPP estimates. For example, the MODIS 8-day vegetation indices (EVI and LSWI) used in VPM model were calculated from 8-day surface reflectance composite data that are generated by the Maximum Value Composite (MVC) or Constrained-View Angle Maximum Value Composite (CV-MVC) algorithm (Chen et al., 2006; Huete et al., 2002). MODIS surface reflectance data are often affected by cloud, snow, and soil background (Chang et al., 2019; Huete et al., 2002). Contaminated or missing observations were gap-filled using simple linear regression model or non-linear regression model such as S-G fitting method (Chang et al., 2018). However, the gap-filling procedures can lead to an underestimation of FPAR or LUE and subsequently introduced considerable error to the GPP product (Zhao et al., 2005). EVI still has limitations in capturing the seasonal dynamics of dense canopies (Chang et al., 2019), which could result in the underestimation of GPP in ENF and EBF.

5. Conclusions

Biome-specific parameters have introduced errors and uncertainties in GPP simulation. Here, we assessed the consistency of $\mathbf{T_{opt-b-EC}}$, $\mathbf{T_{opt-s}}$, $\mathbf{T_{opt-sy}}$, and $\mathbf{T_{opt-b-LT}}$ and their effects on satellite-based GPP estimates. Our use of an accumulated temperature-based growing season efficiently decreased the effects of snow on $\mathbf{T_{opt}}$ estimation. We explored the use of MODIS EVI to approximate $\mathbf{T_{opt}}$ of photosynthesis and found that $\mathbf{T_{opt-b}}$, $\mathbf{T_{opt-s}}$, and $\mathbf{T_{opt-sy}}$ from EVI were significantly close to those from GPP_{EC}. We calculated site-level GPP_{VPM} by using $\mathbf{T_{opt-b-LT}}$, $\mathbf{T_{opt-b-EC}}$, and $\mathbf{T_{opt-sy-EVI}}$. The new GPP_{VPM} estimates, especially GPP with $\mathbf{T_{opt-sy-EVI}}$, significantly improved GPP_{VPM} estimates. We used 165 flux sites distributed globally and in various biomes, which indicated that the method can be used in regional and global scale. The relationship between biome-specific, site-specific, and site-year-specific temperature with improved GPP estimates can help in carbon-related agriculture, environment, health, and economic decision-making.

Declaration of Competing Interest

The authors declare that they have no known competing financial interests or personal relationships that could have appeared to influence the work reported in this paper.

Acknowledgement

This study was supported in part by research grants from the USDA National Institute of Food and Agriculture (NIFA) (2016-68002-24967) and the U.S. National Science Foundation (IIA-1920946, IIA-1946093, EEID-1911955). The eddy covariance data used in this study was acquired and shared by the FLUXNET community, including the following networks: AmeriFlux, AfriFlux, AsiaFlux, CarboAfrica, CarboEuropeIP, CarboItaly, CarboMont, ChinaFlux, Fluxnet-Canada, GreenGrass, ICOS, KoFlux, LBA, NECC, OzFlux-TERN, TCOS-Siberia, and USCCC. We thank the reviewers for their time and effort in reviewing this manuscript and their comments and suggestions substantially improve this manuscript.

Appendix. Supplementary materials

Download : **Download Word document (3MB)**

Recommended articles Citing articles (0)

References

Anav et al., 2015 A. Anav, *et al.*
. Spatiotemporal patterns of terrestrial gross primary production: A review
Reviews of Geophysics, 53 (3) (2015), pp. 785-818
View Record in Scopus Google Scholar

Badgley et al., 2017 G. Badgley, C.B. Field, J.A. Berry
Canopy near-infrared reflectance and terrestrial photosynthesis
Science Advances, 3 (3) (2017), Article e1602244
CrossRef View Record in Scopus Google Scholar

Baldocchi, 2003 D.D. Baldocchi
Assessing the eddy covariance technique for evaluating carbon dioxide exchange rates of ecosystems: past, present and future
Global change biology, 9 (4) (2003), pp. 479-492
CrossRef View Record in Scopus Google Scholar

Battin et al., 2009 T.J. Battin, *et al.*
The boundless carbon cycle
Nature Geoscience, 2 (9) (2009), p. 598
CrossRef View Record in Scopus Google Scholar

Chandrasekar et al., 2010 K. Chandrasekar, M. Sesha Sai, P. Roy, R. Dwevedi
Land Surface Water Index (LSWI) response to rainfall and NDVI using the MODIS Vegetation Index product
International Journal of Remote Sensing, 31 (15) (2010), pp. 3987-4005
CrossRef View Record in Scopus Google Scholar

Chang et al., 2019 Q. Chang, *et al.*
Assessing consistency of spring phenology of snow-covered forests as estimated by vegetation indices, gross primary production, and solar-induced chlorophyll fluorescence
Agricultural and Forest Meteorology, 275 (2019), pp. 305-316
Article Download PDF View Record in Scopus Google Scholar

Chang et al., 2020 Q. Chang, *et al.*
Estimating site-specific optimum air temperature and assessing its effect on the photosynthesis of grasslands in mid-to high-latitudes
Environmental Research Letters, 15 (3) (2020), Article 034064

CrossRef View Record in Scopus Google Scholar

Chang et al., 2018 Q. Chang, J. Zhang, W. Jiao, F. Yao
A comparative analysis of the NDVIg and NDVI3g in monitoring vegetation phenology changes in the Northern Hemisphere
Geocarto international, 33 (1) (2018), pp. 1-20
View Record in Scopus Google Scholar

Chen et al., 2006 P.-Y. Chen, G. Fedosejevs, M. Tiscareno-Lopez, J.G. Arnold
Assessment of MODIS-EVI, MODIS-NDVI and VEGETATION-NDVI composite data using agricultural measurements: An example at corn fields in western Mexico
Environmental monitoring and assessment, 119 (1-3) (2006), pp. 69-82
CrossRef View Record in Scopus Google Scholar

Durgun et al., 2016 Y.Ö. Durgun, A. Gobin, S. Gilliams, G. Duveiller, B. Tychon
Testing the contribution of stress factors to improve wheat and maize yield estimations derived from remotely-sensed dry matter productivity
Remote Sensing, 8 (3) (2016), p. 170
CrossRef View Record in Scopus Google Scholar

Fitter and Hay, 2012 A.H. Fitter, R.K. Hay
Environmental physiology of plants
Academic press (2012)
Google Scholar

Fridley et al., 2016 J.D. Fridley, J.S. Lynn, J. Grime, A. Askew
Longer growing seasons shift grassland vegetation towards more-productive species
Nature Climate Change, 6 (9) (2016), p. 865
CrossRef View Record in Scopus Google Scholar

Friedl et al., 2002 M.A. Friedl, *et al.*
Global land cover mapping from MODIS: algorithms and early results
Remote Sensing of Environment, 83 (1-2) (2002), pp. 287-302
Article Download PDF View Record in Scopus Google Scholar

Gamon et al., 2013 J.A. Gamon, K.F. Huemmrich, R.S. Stone, C.E. Tweedie
Spatial and temporal variation in primary productivity (NDVI) of coastal Alaskan tundra: Decreased vegetation growth following earlier snowmelt
Remote sensing of environment, 129 (2013), pp. 144-153
Article Download PDF View Record in Scopus Google Scholar

Haberl et al., 2007 H. Haberl, *et al.*
Quantifying and mapping the human appropriation of net primary production in earth's terrestrial ecosystems
Proceedings of the National Academy of Sciences, 104 (31) (2007), pp. 12942-12947
CrossRef View Record in Scopus Google Scholar

Heinsch et al., 2006 F.A. Heinsch, *et al.*
Evaluation of remote sensing based terrestrial productivity from MODIS using regional tower eddy flux network observations
IEEE Transactions on Geoscience and Remote Sensing, 44 (7) (2006), pp. 1908-1925
CrossRef Google Scholar

Hovenden et al., 2014 M.J. Hovenden, P.C. Newton, K.E. Wills
Seasonal not annual rainfall determines grassland biomass response to carbon dioxide
Nature, 511 (7511) (2014), p. 583

CrossRef View Record in Scopus Google Scholar

Huang et al., 2018 K. Huang, *et al.*
Enhanced peak growth of global vegetation and its key mechanisms
Nature ecology & evolution, 2 (12) (2018), p. 1897
CrossRef View Record in Scopus Google Scholar

Huang et al., 2019 M. Huang, *et al.*
Air temperature optima of vegetation productivity across global biomes
Nature Ecology & Evolution, 1 (2019)
Google Scholar

Huete et al., 2002 A. Huete, *et al.*
Overview of the radiometric and biophysical performance of the MODIS vegetation indices
Remote Sens Environ, 83 (1) (2002), pp. 195-213
Article Download PDF View Record in Scopus Google Scholar

Hufkens et al., 2016 K. Hufkens, *et al.*
Productivity of North American grasslands is increased under future climate scenarios despite rising aridity
Nature Climate Change, 6 (7) (2016), p. 710
CrossRef View Record in Scopus Google Scholar

Jiao et al., 2019 W. Jiao, Q. Chang, L. Wang
The Sensitivity of Satellite Solar-Induced Chlorophyll Fluorescence to Meteorological Drought
Earth's Future, 7 (5) (2019), pp. 558-573
View Record in Scopus Google Scholar

Kanniah et al., 2009 K.D. Kanniah, J. Beringer, L.B. Hutley, N.J. Tapper, X. Zhu
Evaluation of Collections 4 and 5 of the MODIS Gross Primary Productivity product and algorithm improvement at a tropical savanna site in northern Australia
Remote Sensing of Environment, 113 (9) (2009), pp. 1808-1822
Article Download PDF View Record in Scopus Google Scholar

King et al., 2011 D.A. King, D.P. Turner, W.D. Ritts
Parameterization of a diagnostic carbon cycle model for continental scale application
Remote Sensing of Environment, 115 (7) (2011), pp. 1653-1664
Article Download PDF View Record in Scopus Google Scholar

Larcher, 1980 W. Larcher
Physiological plant ecology
(Second edition), Springer-Verg, Berlin, West Germany (1980)
Google Scholar

Lin et al., 2012 Y.-S. Lin, B.E. Medlyn, D.S. Ellsworth
Temperature responses of leaf net photosynthesis: the role of component processes
Tree Physiology, 32 (2) (2012), pp. 219-231
CrossRef View Record in Scopus Google Scholar

Ma et al., 2014 X. Ma, *et al.*
Parameterization of an ecosystem light-use-efficiency model for predicting savanna GPP using MODIS EVI
Remote Sensing of Environment, 154 (2014), pp. 253-271
Article Download PDF View Record in Scopus Google Scholar

McGuire et al., 1992 A.D. McGuire, *et al.*
Interactions between carbon and nitrogen dynamics in estimating net primary productivity for potential vegetation in North America

Global Biogeochemical Cycles, 6 (2) (1992), pp. 101-124
View Record in Scopus Google Scholar

Melillo et al., 1993 J.M. Melillo, *et al.*
Global climate change and terrestrial net primary production
Nature, 363 (6426) (1993), p. 234
CrossRef View Record in Scopus Google Scholar

Monteith, 1972 J.L. Monteith
Solar radiation and productivity in tropical ecosystems
Journal of applied ecology, 9 (3) (1972), pp. 747-766
CrossRef Google Scholar

Monteith, 1977 J.L. Monteith
Climate and the efficiency of crop production in Britain
Phil. Trans. R. Soc. Lond. B, 281 (980) (1977), pp. 277-294
Google Scholar

Niu et al., 2012 S. Niu, *et al.*
Thermal optimality of net ecosystem exchange of carbon dioxide and underlying mechanisms
New Phytologist, 194 (3) (2012), pp. 775-783
CrossRef View Record in Scopus Google Scholar

Papale et al., 2006 D. Papale, *et al.*
Towards a standardized processing of Net Ecosystem Exchange measured with eddy covariance technique: algorithms and uncertainty estimation
Biogeosciences, 3 (4) (2006), pp. 571-583
CrossRef View Record in Scopus Google Scholar

Pei et al., 2018 Y. Pei, J. Huang, L. Wang, H. Chi, Y. Zhao
An improved phenology-based CASA model for estimating net primary production of forest in central China based on Landsat images
International Journal of Remote Sensing (2018), pp. 1-29
View Record in Scopus Google Scholar

Potter et al., 2003 C. Potter, *et al.*
Continental-scale comparisons of terrestrial carbon sinks estimated from satellite data and ecosystem modeling 1982–1998
Glob. Planet. Change, 39 (3-4) (2003), pp. 201-213
Article Download PDF View Record in Scopus Google Scholar

Prentice et al., 1992 I.C. Prentice, *et al.*
Special paper: a global biome model based on plant physiology and dominance, soil properties and climate
Journal of biogeography (1992), pp. 117-134
CrossRef View Record in Scopus Google Scholar

Prince and Goward, 1995 S.D. Prince, S.N. Goward
Global primary production: a remote sensing approach
Journal of biogeography (1995), pp. 815-835
CrossRef View Record in Scopus Google Scholar

Raich et al., 1991 J.W. Raich, *et al.*
Potential net primary productivity in South America: application of a global model
Ecological Applications, 1 (4) (1991), pp. 399-429
CrossRef View Record in Scopus Google Scholar

Reichstein et al., 2005 M. Reichstein, *et al.*

On the separation of net ecosystem exchange into assimilation and ecosystem respiration: review and improved algorithm

Global Change Biology, 11 (9) (2005), pp. 1424-1439

CrossRef View Record in Scopus Google Scholar

Reichstein et al., 2007 M. Reichstein, *et al.*

Determinants of terrestrial ecosystem carbon balance inferred from European eddy covariance flux sites

Geophysical Research Letters, 34 (1) (2007)

Google Scholar

Running et al., 1999 S.W. Running, *et al.*

A global terrestrial monitoring network integrating tower fluxes, flask sampling, ecosystem modeling and EOS satellite data

Remote sensing of environment, 70 (1) (1999), pp. 108-127

Article Download PDF View Record in Scopus Google Scholar

Running and Zhao, 2015 S.W. Running, M. Zhao

Daily GPP and annual NPP (MOD17A2/A3) products NASA Earth Observing System MODIS land algorithm

MOD17 User's Guide (2015)

Google Scholar

Ryu et al., 2019 Y. Ryu, J.A. Berry, D.D. Baldocchi

What is global photosynthesis? History, uncertainties and opportunities

Remote Sensing of Environment, 223 (2019), pp. 95-114

Article Download PDF View Record in Scopus Google Scholar

Schaefer et al., 2012 K. Schaefer, *et al.*

A model-data comparison of gross primary productivity: Results from the North American Carbon Program site synthesis

Journal of Geophysical Research: Biogeosciences, 117 (G3) (2012)

Google Scholar

Sitch et al., 2008 S. Sitch, *et al.*

Evaluation of the terrestrial carbon cycle, future plant geography and climate-carbon cycle feedbacks using five Dynamic Global Vegetation Models (DGVMs)

Global Change Biology, 14 (9) (2008), pp. 2015-2039

CrossRef View Record in Scopus Google Scholar

Sjöström et al., 2013 M. Sjöström, *et al.*

Evaluation of MODIS gross primary productivity for Africa using eddy covariance data

Remote Sensing of Environment, 131 (2013), pp. 275-286

Article Download PDF View Record in Scopus Google Scholar

Smith et al., 2016 N.G. Smith, S.L. Malyshev, E. Shevliakova, J. Kattge, J.S. Dukes

Foliar temperature acclimation reduces simulated carbon sensitivity to climate

Nature Climate Change, 6 (4) (2016), pp. 407-411

CrossRef View Record in Scopus Google Scholar

Stocker et al., 2019 B.D. Stocker, *et al.*

Drought impacts on terrestrial primary production underestimated by satellite monitoring

Nature Geoscience, 1 (2019)

Google Scholar

Turner et al., 2006a D. Turner, *et al.*

A diagnostic carbon flux model to monitor the effects of disturbance and interannual variation in climate on regional NEP
Tellus B: Chemical and Physical Meteorology, 58 (5) (2006), pp. 476-490
CrossRef View Record in Scopus Google Scholar

Turner et al., 2006b D.P. Turner, *et al.*
Evaluation of MODIS NPP and GPP products across multiple biomes
Remote Sensing of Environment, 102 (3-4) (2006), pp. 282-292
Article Download PDF View Record in Scopus Google Scholar

Tutmez, 2006 B. Tutmez
Trend analysis for the projection of energy-related carbon dioxide emissions
Energy exploration & exploitation, 24 (1-2) (2006), pp. 139-149
CrossRef Google Scholar

Veroustraete et al., 2002 F. Veroustraete, H. Sabbe, H. Eerens
Estimation of carbon mass fluxes over Europe using the C-Fix model and Euroflux data
Remote Sensing of Environment, 83 (3) (2002), pp. 376-399
Article Download PDF View Record in Scopus Google Scholar

Wang et al., 2018 X. Wang, C. Wu, D. Peng, A. Gonsamo, Z. Liu
Snow cover phenology affects alpine vegetation growth dynamics on the Tibetan Plateau: Satellite observed evidence, impacts of different biomes, and climate drivers
Agricultural and Forest Meteorology, 256 (2018), pp. 61-74
Article Download PDF CrossRef View Record in Scopus Google Scholar

Waring et al., 1995 R. Waring, *et al.*
Scaling gross ecosystem production at Harvard Forest with remote sensing: a comparison of estimates from a constrained quantum-use efficiency model and eddy correlation
Plant, Cell & Environment, 18 (10) (1995), pp. 1201-1213
CrossRef View Record in Scopus Google Scholar

Wu et al., 2018a C. Wu, *et al.*
Contrasting responses of autumn-leaf senescence to daytime and night-time warming
Nature Climate Change, 9 (2) (2018), p. 177
View Record in Scopus Google Scholar

Wu et al., 2018b X. Wu, *et al.*
Spatiotemporal consistency of four gross primary production products and solar-induced chlorophyll fluorescence in response to climate extremes across CONUS in 2012
Journal of Geophysical Research: Biogeosciences (2018)
Google Scholar

Xiao et al., 2014 J. Xiao, K.J. Davis, N.M. Urban, K. Keller
Uncertainty in model parameters and regional carbon fluxes: A model-data fusion approach
Agricultural and Forest Meteorology, 189 (2014), pp. 175-186
Article Download PDF View Record in Scopus Google Scholar

Xiao et al., 2011 J. Xiao, K.J. Davis, N.M. Urban, K. Keller, N.Z. Saliendra
Upscaling carbon fluxes from towers to the regional scale: Influence of parameter variability and land cover representation on regional flux estimates
Journal of Geophysical Research: Biogeosciences, 116 (G3) (2011)
Google Scholar

Xiao et al., 2009 X. Xiao, C.M. Biradar, C. Czarnecki, T. Alabi, M. Keller

A simple algorithm for large-scale mapping of evergreen forests in tropical America, Africa and Asia
Remote Sensing, 1 (3) (2009), pp. 355-374
CrossRef View Record in Scopus Google Scholar

Xiao et al., 2004 X. Xiao, *et al.*
Modeling gross primary production of temperate deciduous broadleaf forest using satellite images and climate data
Remote Sensing of Environment, 91 (2) (2004), pp. 256-270
Article Download PDF View Record in Scopus Google Scholar

Yan et al., 2019 D. Yan, R. Scott, D. Moore, J. Biederman, W. Smith
Understanding the relationship between vegetation greenness and productivity across dryland ecosystems through the integration of PhenoCam, satellite, and eddy covariance data
Remote sensing of environment, 223 (2019), pp. 50-62
Article Download PDF View Record in Scopus Google Scholar

Yan et al., 2015 H. Yan, *et al.*
Improved global simulations of gross primary product based on a new definition of water stress factor and a separate treatment of C3 and C4 plants
Ecological modelling, 297 (2015), pp. 42-59
Article Download PDF View Record in Scopus Google Scholar

Yang et al., 2019 J. Yang, *et al.*
Divergent shifts in peak photosynthesis timing of temperate and alpine grasslands in China
Remote Sensing of Environment, 233 (2019), Article 111395
Article Download PDF View Record in Scopus Google Scholar

Yuan et al., 2007 W. Yuan, *et al.*
Deriving a light use efficiency model from eddy covariance flux data for predicting daily gross primary production across biomes
Agricultural and Forest Meteorology, 143 (3-4) (2007), pp. 189-207
Article Download PDF View Record in Scopus Google Scholar

Zhang et al., 2014 Q. Zhang, *et al.*
Estimation of crop gross primary production (GPP): fAPARchl versus MOD15A2 FPAR
Remote Sensing of Environment, 153 (2014), pp. 1-6
Article Download PDF CrossRef View Record in Scopus Google Scholar

Zhang et al., 2013 Q. Zhang, E.M. Middleton, Y.-B. Cheng, D.R. Landis
Variations of Foliage Chlorophyll fAPAR and Foliage Non-Chlorophyll fAPAR (fAPAR $ _ {\rm chl} $, fAPAR $ _ {\rm non\mathchar" 702D chl} $) at the Harvard Forest
IEEE Journal of Selected Topics in Applied Earth Observations and Remote Sensing, 6 (5) (2013), pp. 2254-2264
CrossRef View Record in Scopus Google Scholar

Zhang et al., 2009 Q. Zhang, *et al.*
Can a satellite-derived estimate of the fraction of PAR absorbed by chlorophyll (FAPARchl) improve predictions of light-use efficiency and ecosystem photosynthesis for a boreal aspen forest?
Remote Sensing of Environment, 113 (4) (2009), pp. 880-888
Article Download PDF View Record in Scopus Google Scholar

Zhang et al., 2016 Y. Zhang, *et al.*
Consistency between sun-induced chlorophyll fluorescence and gross primary production of vegetation in North America
Remote Sensing of Environment, 183 (2016), pp. 154-169
Article Download PDF CrossRef View Record in Scopus Google Scholar

Zhang et al., 2017 Y. Zhang, *et al.*

A global moderate resolution dataset of gross primary production of vegetation for 2000–2016

Scientific data, 4 (2017), Article 170165

View Record in Scopus Google Scholar

Zhao et al., 2005 M. Zhao, F.A. Heinsch, R.R. Nemani, S.W. Running

Improvements of the MODIS terrestrial gross and net primary production global data set

Remote sensing of Environment, 95 (2) (2005), pp. 164-176

Article Download PDF View Record in Scopus Google Scholar

Zhao and Running, 2010 M. Zhao, S.W. Running

Drought-induced reduction in global terrestrial net primary production from 2000 through 2009

science, 329 (5994) (2010), pp. 940-943

CrossRef View Record in Scopus Google Scholar

Zheng et al., 2018 Y. Zheng, *et al.*

Sources of uncertainty in gross primary productivity simulated by light use efficiency models: Model structure, parameters, input data, and spatial resolution

Agricultural and forest meteorology, 263 (2018), pp. 242-257

Article Download PDF View Record in Scopus Google Scholar

Zhu et al., 2018 X. Zhu, *et al.*

Underestimates of Grassland Gross Primary Production in MODIS Standard Products

Remote Sensing, 10 (11) (2018), p. 1771

CrossRef View Record in Scopus Google Scholar

View Abstract